J|A|C|S ARTICLES

Published on Web 09/18/2009

Swallow-Tail Substituted Liquid Crystalline Perylene Bisimides: Synthesis and Thermotropic Properties

André Wicklein, Andreas Lang, Mathis Muth, and Mukundan Thelakkat*

Department of Macromolecular Chemistry I, Applied Functional Polymers, Universität Bayreuth, Universitätsstraβe 30, 95440 Bayreuth, Germany

Received June 26, 2009; E-mail: mukundan.thelakkat@uni-bayreuth.de

Abstract: Tailor-made synthesis and structure−property relationship of several swallow-tail *N*-substituted perylene bisimide (PBI) dyes are presented. PBI derivatives were synthesized by two distinct synthetic approaches, the details being evaluated herein. All the PBIs carry either alkyl swallow-tail or oligoethylenglycolether (OEG) swallow-tail moieties as *N*-substituents, and many of them are unsymmetrically substituted. We avoided substitution at bay positions of the perylene core to maintain the planarity and strong $\pi-\pi$ interactions, which favor intermolecular order and charge carrier transport. The thermotropic behavior, which is strongly influenced by the nature of the substituents was investigated using differential scanning calorimetry (DSC), polarization optical microscopy (POM), and X-ray diffraction measurements (XRD). The introduction of OEG swallow-tail units facilitates thermotropic liquid crystalline behavior in most cases and the unsymmetrical substitution allowed the tuning of the mesophase-width. The mesophases exhibit characteristic columnar hexagonal (Col_h) packing arising from $\pi-\pi$ interactions between cofacially orientated perylene molecules. Thus, the inherent tendency of PBI molecules for crystallization could be effectively suppressed by incorporating flexible OEG swallow-tail units only at imide positions. This molecular design was crucial to obtain liquid crystallinity and intracolumnar long-range order. The substituents did not influence the electronic energy levels such as HOMO and LUMO.

Introduction

Perylene bisimide[1,2] (PBI, perylene tetracarboxylic acid bisimide) derivatives represent an important class of n-type semiconductor materials exhibiting a relatively high electron affinity among large-band gap materials.[3−5] PBIs are readily available inexpensive robust compounds, and they combine high quantum yields of photoluminescence with excellent photochemical and thermal stability.[6,7] PBIs are promising compounds for application in organic electronic devices.[8−11] The solid-state packing of the perylene bisimides determines the morphology in thin films, which plays a major role in improving the device performance. For instance, an increase in exciton diffusion length and an improvement in charge carrier mobilities can be achieved by increased ordering of PBI molecules.[12,13] In general, inducing liquid crystallinity is an elegant way of improving supramolecular organization, as it promotes $\pi-\pi$ stacking, allows for dynamic reorganization, and facilitates the processing of thin films, which is not feasible with highly crystalline materials.[14−17] The unique structural and electronic properties of especially discotic liquid crystals,[18,19] also open completely different aspects of possible applications in topical research fields such as molecular electronics and high-efficiency organic photovoltaics.[8,20−22] Most semiconducting discotics are good hole transporting materials (p-type), while only a limited number

(1) Würthner, F. *Chem. Commun.* **2004**, 1564–1579.
(2) Langhals, H. *Helv. Chim. Acta* **2005**, *88*, 1309–1343.
(3) Struijk, C. W.; Sieval, A. B.; Dakhorst, J. E. J.; van Dijk, M.; Kimkes, P.; Koehorst, R. B. M.; Donker, H.; Schaafsma, T. J.; Picken, S. J.; van de Craats, A. M.; Warman, J. M.; Zuilhof, H.; Sudholter, E. J. R. *J. Am. Chem. Soc.* **2000**, *122*, 11057–11066.
(4) Horowitz, G.; Kouki, F.; Spearman, P.; Fichou, D.; Nogues, C.; Pan, X.; Garnier, F. *Adv. Mater.* **1996**, *8*, 242–245.
(5) Dimitrakopoulos, C. D.; Malenfant, P. R. L. *Adv. Mater.* **2002**, *14*, 99–117.
(6) Jancy, B.; Asha, S. K. *J. Phys. Chem. B* **2006**, *110*, 20937–20947.
(7) Geissler, G.; Remy, H. (Hoechst AG), *Ger. Pat. Appl.*, DE 1130099, October 24, 1959.
(8) Schmidt-Mende, L.; Fechtenkötter, A.; Müllen, K.; Moons, E.; Friend, R. H.; MacKenzie, J. D. *Science* **2001**, *293*, 1119–1122.
(9) Yakimov, A.; Forrest, S. R. *Appl. Phys. Lett.* **2002**, *80*, 1667–1669.
(10) Lindner, S. M.; Huettner, S.; Chiche, A.; Thelakkat, M.; Krausch, G. *Angew. Chem., Int. Ed.* **2006**, *45*, 3364–3368.
(11) Sommer, M.; Lindner, S. M.; Thelakkat, M. *Adv. Funct. Mater.* **2007**, *17*, 1493–1500.
(12) Löhmannsröben, H. G.; Langhals, H. *Appl. Phys. B: Laser Opt.* **1989**, *48*, 449–452.
(13) Liu, S.-G.; Sui, G.; Cormier, R. A.; Leblanc, R. M.; Gregg, B. A. *J. Phys. Chem. B* **2002**, *106*, 1307–1315.
(14) Simpson, C. D.; Wu, J.; Watson, M. D.; Muellen, K. *J. Mater. Chem.* **2004**, *14*, 494–504.
(15) An, Z.; Yu, J.; Jones, S. C.; Barlow, S.; Yoo, S.; Domercq, B.; Prins, P.; Siebbeles, L. D. A.; Kippelen, B.; Marder, S. R. *Adv. Mater.* **2005**, *17*, 2580–2583.
(16) Kato, T.; Mizoshita, N.; Kishimoto, K. *Angew. Chem., Int. Ed.* **2006**, *45*, 38–68.
(17) Hoeben, F. J. M.; Jonkheijm, P.; Meijer, E. W.; Schenning, A. P. H. J. *Chem. Rev.* **2005**, *105*, 1491–1546.
(18) Laschat, S.; Baro, A.; Steinke, N.; Giesselmann, F.; Haegele, C.; Scalia, G.; Judele, R.; Kapatsina, E.; Sauer, S.; Schreivogel, A.; Tosoni, M. *Angew. Chem., Int. Ed.* **2007**, *46*, 4832–4887.
(19) Destrade, C.; Foucher, P.; Gasparoux, H.; Nguyen, H. T.; Levelut, A. M.; Malthete, J. *Mol. Cryst. Liq. Cryst.* **1984**, *106*, 121–146.
(20) Kopitzke, J.; Wendorff, J. H. *Chem. Unserer Zeit* **2000**, *34*, 4–16.
(21) Nelson, J. *Science* **2001**, *293*, 1059–1060.
(22) Sergeyev, S.; Pisula, W.; Geerts, Y. H. *Chem. Soc. Rev.* **2007**, *36*, 1902–1929.

10.1021/ja905260c CCC: $40.75

of good electron transporting materials (n-type) have been reported.[23]

In general, the self-assembly process of PBI in bulk is a complex balance between molecular stacking arising from $\pi-\pi$ interaction of the perylene core moiety and the flexible nature of appropriate side chains. Thus an optimum balance of rigidy and flexibility that is crucial for inducing liquid crystallinity has to be found. For electronic device applications, the side chains also should be favorably small, so that the dilution of the electronically active perylene moiety with the electronically inactive, insulating side groups is minimal. Hence, a compromise between active chromophore content and side groups that influence the morphology has to be met.

To the best of our knowledge, all of the thermotropic liquid crystalline perylene bisimide derivatives reported in literature are symmetrically substituted. Cormier and Gregg report on liquid crystalline PBIs with branched propylimid-oligo(oxyethylene) or phenethylimide-oligo(oxyethylene) side-chains.[24,25] Pioneering work of Würthner and co-workers involves columnar hexagonal PBIs, with tridodecylphenyl or tridodecyloxyphenyl substituents, also in combination with perylene bay substitution.[26,27] Other reports on symmetrically substituted liquid crystalline PBIs deal with tridodecyloxy gallic acid substituted derivatives[6,28] and PBIs with simple aliphatic chains.[3] Very recently Müllen et al. reported on cooperative molecular motion phenomenon within a symmetrically substituted PBI exhibiting liquid crystalline properties.[29] It has been observed that for various phthalocyanines and triphenylenes, an unsymmetrical substitution pattern broadens the mesophase and strongly influences liquid crystalline packing.[20,30,31] But this has not been studied in the case of PBIs. In fact there are no unsymmetrically *N*-substituted liquid crystalline PBIs published up to date and therefore, this substitution pattern is also investigated here.

A fundamental question here is, how to efficiently weaken the strong degree of crystallinity which is inherent in PBIs using a suitable synthetic strategy for unsymmetrical *N*-substitution. We report here our successful approach of swallow-tail *N*-substitution employing oligoethylenglycol units (OEG) to accomplish this goal. Thus we report for the first time a systematic study on the effect of an asymmetric *N*-substitution pattern of PBIs on the thermotropic behavior. The present approach is aimed at understanding the molecular design requirements to introduce liquid crystalline phases in PBIs without any bay substitution. It can be expected that by introducing two swallow-tail *N*-side chains having different spatial dimensions and additionally different polarities, the thermotropic behavior of PBIs may be tailored. Furthermore, alkyl swallow-tail groups are well-known to induce high solubility in perylene bisimides which allows for the fabrication of solution-processable devices.[32,33] A change from alkyl to oligooxyethylene substituents provides higher conformational flexibility of the C−O bond compared to the C−C bond. Other physical properties, such as optical or redox properties should not be affected by *N*-substitution, as the nodes in the HOMO and LUMO at the imide nitrogen reduce electronic coupling of the perylene bisimide core and the imide substituents to a minimum.[34] This is extremely advantageous if only the thermotropic properties of PBIs should be tailored without altering the electronic properties.

For this purpose, three different types of *N*-substitution patterns were studied (Scheme 1): type I with a symmetric substitution pattern, utilizing different alkyl or OEG swallow-tail substituents. This approach is used to study the influence of substituents with different spatial requirements or polarity on thermotropic behavior of symmetrically *N*-substituted PBIs. Type II uses an unsymmetrical substitution pattern comprising different alkyl swallow-tail substituents in combination with OEG swallow-tail or alkyl swallow-tail with distinct spatial demands. Here an asymmetric substitution is used to study the impact of asymmetry of the substitution profile on thermotropic behavior. Type III consists of unsymmetrical substitution pattern, utilizing swallow-tail in combination with linear alkyl or OEG substituents. Here the influence of a reduction of branched swallow-tail substituents to linear ones is investigated.

Results And Discussion

Synthesis. An overview of the synthesized PBIs **1** to **11** is given in Scheme 1 and the respective synthetic pathway in Scheme 2. The synthesis of PBIs **1**−**11** is based on perylene-3,4,9,10-tetracarboxylic dianhydride **PTCDA** as starting material.

Generally two different synthetic strategies are feasible for asymmetric *N*-substitution of PBIs (Scheme 2, Route A and B). The common method consists of the condensation of monoimides **12** as key intermediates with some primary amine to unsymmetrical PBIs (Route A).[35,36] Generally, condensation reaction of the dianhydride **PTCDA** with excess of primary amines in molten imidazole or quinoline and zinc acetate as Lewis acid catalyst exclusively allows access to symmetrical bisimides (**1**−**4**) in high yields but not to key monoimide intermediates **12**. Even substoichometric amounts of amines usually result in the formation of symmetric bisimides and unreacted perylene dianhydride **PTCDA**. Likewise, the utilization of a mixture of primary amines provides a mixture of two symmetric and one unsymmetric perylene bisimide that is hardly to separate.[35] Nagao and Misono depict a partial saponification of the symmetric bisimides to monoimides **12** with conc. sulphuric acid at high temperatures.[37,38] On the other hand, Langhals describes a partial saponification under strong basic conditions with KOH in *t*-BuOH as reaction medium.[35] In the following, we prepared PBIs **1**−**4** and **6**−**9** using Route A, by saponification of bisimides with KOH and subsequent condensation with a second amine. Additionally a microwave-assisted

(23) Chesterfield, R. J.; McKeen, J. C.; Newman, C. R.; Ewbank, P. C.; da Silva Filho, D. A.; Bredas, J.-L.; Miller, L. L.; Mann, K. R.; Frisbie, C. D. *J. Phys. Chem. B* **2004**, *108*, 19281–19292.
(24) Cormier, R. A.; Gregg, B. A. *Chem. Mater.* **1998**, *10*, 1309–1319.
(25) Cormier, R. A.; Gregg, B. A. *J. Phys. Chem. B* **1997**, *101*, 11004–11006.
(26) Würthner, F.; Thalacker, C.; Diele, S.; Tschierske, C *Chem.—Eur. J.* **2001**, *7*, 2245–2253.
(27) Chen, Z.; Baumeister, U.; Tschierske, C.; Würthner, F. *Chem. Eur. J.* **2007**, *13*, 450–465.
(28) Jancy, B.; Asha, S. K. *Chem. Mater.* **2008**, *20*, 169–181.
(29) Hansen, M. R.; Schnitzler, T.; Pisula, W.; Graf, R.; Müllen, K.; Spiess, H. W. *Angew. Chem., Int. Ed.* **2009**, *48*, 4621–4624.
(30) Clarkson, G. J.; Cook, A.; McKeown, N. B.; Treacher, K. E.; Ali-Adib, Z. *Macromolecules* **1996**, *29*, 913–917.
(31) Ali-Adib, Z.; Clarkson, G. J.; McKeown, N. B.; Treacher, K. E.; Gleeson, H. F.; Stennett, A. S. *J. Mater. Chem.* **1998**, *8*, 2371–2378.
(32) Langhals, H.; Ismael, R.; Yürük, O. *Tetrahedron* **2000**, *56*, 5435–5441.
(33) Langhals, H.; Demmig, S.; Potrawa, T. *J. Prakt. Chem.* **1991**, *333*, 733–748.
(34) Langhals, H.; Demmig, S.; Huber, H. *Spectrochim. Acta A* **1988**, *44A*, 1189–1193.
(35) Kaiser, H.; Lindner, J.; Langhals, H. *Chem. Ber.* **1991**, *124*, 529–535.
(36) Langhals, H.; Saulich, S. *Chem. Eur. J.* **2002**, *8*, 5630–5643.
(37) Nagao, Y.; Misono, T. *Dyes Pigm.* **1984**, *5*, 171–188.
(38) Nagao, Y.; Misono, T. *Bull. Chem. Soc. Jpn.* **1981**, *54*, 1191–1194.

Scheme 1. Overview of Symmetrically and Unsymmetrically *N*-Substituted Perylene Bisimides (PBIs) Classified According to the Nature of Respective Substituents[a]

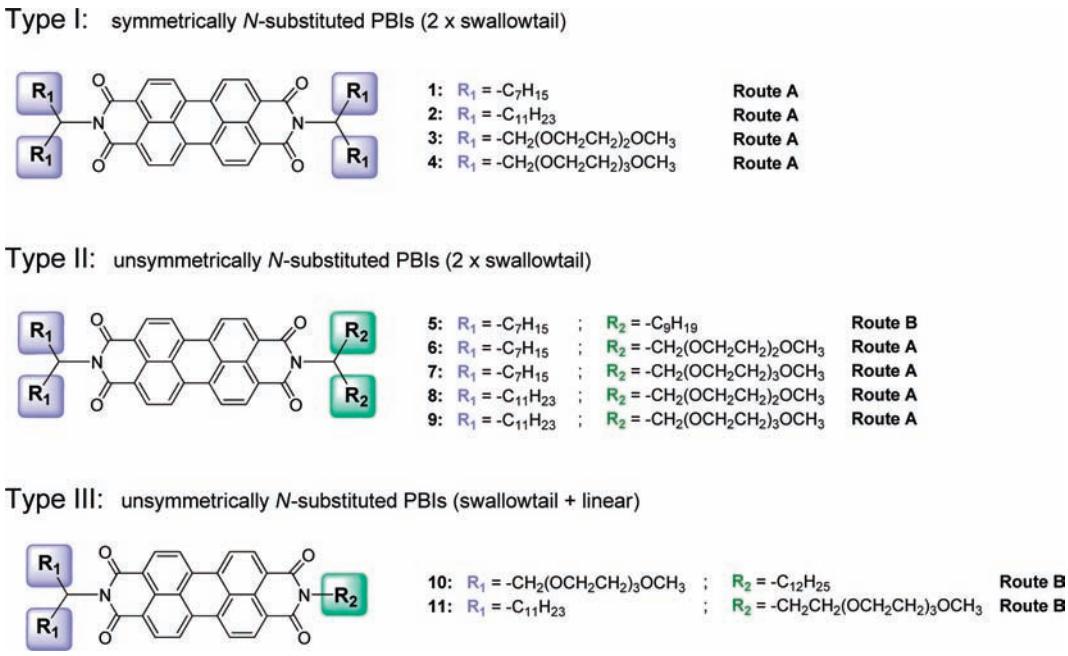

[a] PBIs were prepared either by synthetic route A or B.

Scheme 2. Main Synthetic Pathways for Unsymmetrical *N*-Substitution of Perylene Bisimides[a]

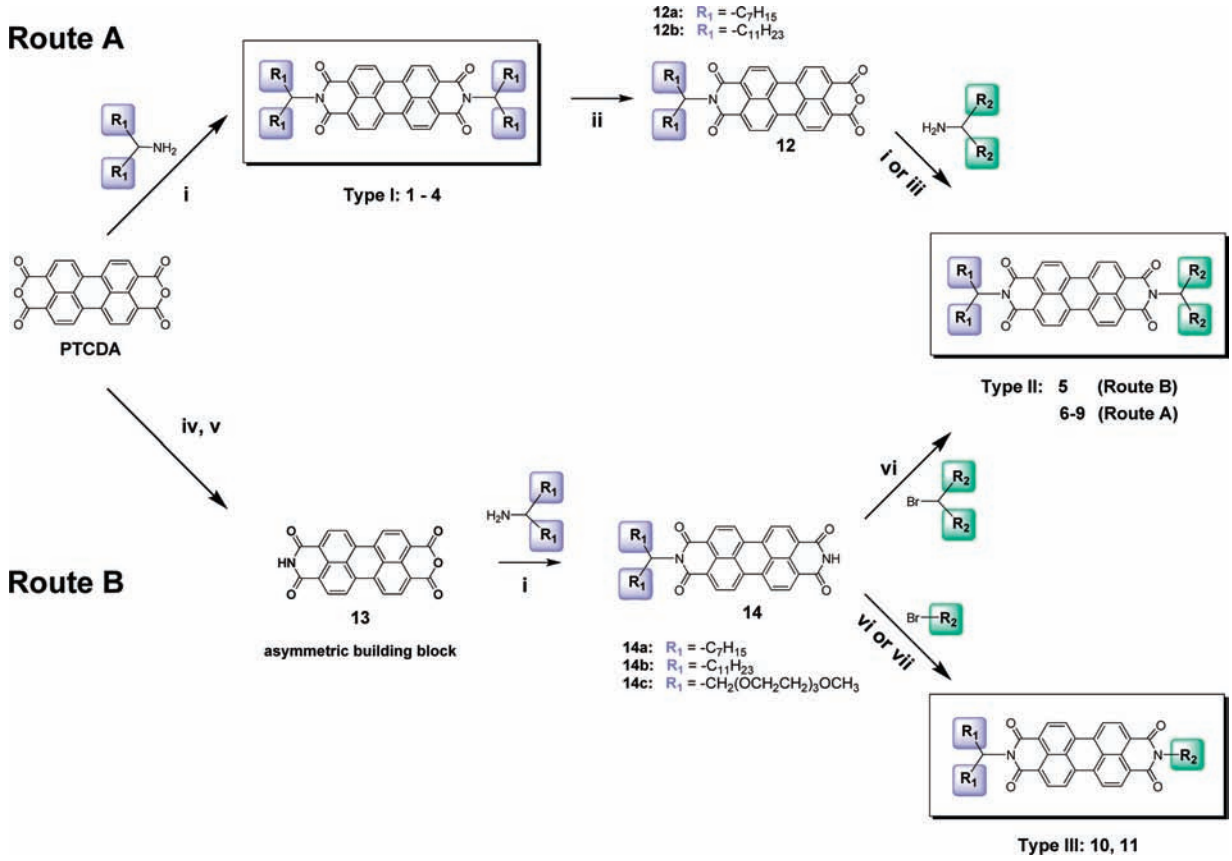

[a] (i) Imidazole, $Zn(OAc)_2$, 2−4 h, 160 °C; (ii) KOH, *t*-BuOH, 90°C 1−1.5 h; (iii) DMAc, $Zn(OAc)_2$, 20 min, 160 °C, 200 W; (iv) 1. KOH, 2. AcOH; (v) NH_4OH, K_2CO_3; (vi) DMF, K_2CO_3, KI, 80 °C, 3−5 d; (vii) DMF, NaH, 80 °C, 48 h. Route A: **1**−**4** and **6**−**9**; Route B: **5**, **10** and **11**.

method for the condensation reaction of monoimide monoanhydride **12** with amines was also developed.

An alternative method (Route B) makes use of imide anhydride **13** as asymmetric building block.[39,40] The anhydride moiety allows for condensation reactions with amines in a first step, whereas the imide moiety offers the possibility for introduction of a second *N*-substituent via nucleophilic substitution S_N2 under basic conditions with alkylhalides in a second

step. Thus Route B employing asymmetric synthon **13** to attain asymmetric *N*-substituted PBIs was pursued as synthetic strategy for PBIs **5**, **10** and **11**.

All the required linear and swallow-tail amines and halides were prepared according to conventional synthetic methods already reported in literature. Alkyl swallow-tail amines were accessible by reductive amination of the corresponding ketones with ammonia and $NaBH_3CN$ as reducing agent in high yields.[41,42] Alkyl swallow-tail bromide was synthesized by bromination of the respective alcohol, which was obtained by a double grignard reaction of the respective alkyl bromide with ethyl formiate.[43] OEG swallow-tail amines were derived by a 4 step sequence: OEG swallow-tail secondary alcohols were prepared according to reported procedures,[44,45] converted to the corresponding tosylates[46,47] and then transformed to the azides by nucleophilic substitution.[48] The azides were finally reduced by $LiAlH_4$ to the corresponding amines. Linear oligooxyethylene-bromides were obtained by bromination of the respective alcohol according to literature procedure.[49]

The symmetrically substituted PBIs **1**−**4** (Type I) were synthesized by simple conversion of perylene dianhydride **PTCDA** with the respective swallow-tail amine (Route A first step). This well-established method allows for high yields of the bisimide products. Due to swallow-tail substituents, the bisimides obtained are highly soluble. For an unsymmetrical substitution, to obtain type II derivatives, the disubstituted PBIs **1** and **2** were partially hydrolyzed to the monoimide monoanhydrides **12a, b** respectively by treatment with an excess KOH in *t*-BuOH. Finally these unsymmetrical alkyl swallow-tail OEG swallow-tail PBIs **6**, **7**, **8** and **9** were obtained by conversion of the respective monoimide monoanhydrides (**12a** or **12b**) with the respective OEG swallow-tail amine. The intermediate **12a** was converted to **6** and **7**, whereas **12b** resulted in **8** and **9**. For this synthetic step, microwave irradiation conditions were applied. Under microwave conditions, the reaction time could be reduced drastically from 4 h to 20 min and high yields were generally obtained (for example, 96% for PBI **6**). On the other hand, unsymmetrically substituted PBIs **5, 10** and **11** were obtained via the asymmetric building block **13** according to Route B. After condensation reaction of **13** with the respective alkyl swallow-tail amine, the second substituent was introduced via nucleophilic substitution using the respective bromide in a subsequent step to get **5**, **10** and **11**. Both synthetic routes allow for satisfactory yields of the final unsymmetrical PBI products, described under type II and III. The advantage of Route B is that it is straightforward and there is no unnecessary loss of side chain amine in the bisimide hydrolysis step. Additionally the comparatively mild reaction conditions (<60 °C) for the nucleophilic substitution allow for introduction of *N*-substituents that are unstable at higher temperatures. A high level of purity was achieved for all PBI compounds by repeated column chromatography purification until they all showed a single chromatogram in gel permeation chromatography (GPC).

All PBIs were fully characterized by means of ^1H, ^{13}C NMR spectroscopy, IR, GPC, MS and Microanalyses. These PBIs can be regarded as a closed chromophoric system due to the nodes of the HOMO and LUMO orbitals at imide nitrogens.[34] Accordingly, the PBIs under investigation with different substituents show identical absorption behavior. The UV−vis spectra of these compounds in very dilute solutions exhibit the characteristic fingerprint vibronic fine structure of PBI with peaks at about 525, 490, 460, and 430 nm respectively. In order to elucidate the electronic energy levels which determine the energy and electron transfer processes, and the reversibility of redox processes, cyclic voltammetry (CV) was used. CV is a common method for studying electrochemical behavior and to evaluate the relative HOMO and LUMO levels using ferrocene as internal calibration. PBIs possess good electron affinity and so they are easy to be reduced and rather difficult to be oxidized. All PBIs investigated herewith, exhibit two reversible reduction peaks. In order to calculate the absolute values of HOMO and LUMO levels, the redox data was calibrated with respect to ferrocene-ferrocenium couple Fc/Fc^+, which has a quasi-calculated HOMO-energy level of 4.8 eV.[50] The LUMO energy levels of PBIs were obtained from the half-wave reduction potentials. However, the oxidation potentials of most compounds were not observed in the CV measurements window up to +1 V vs $Ag/AgNO_3$. Hence the HOMO levels of PBIs were estimated from the optical band gap and the LUMO levels. The optical band gaps of all PBIs were determined from the absorption edge of absorption spectra of diluted solutions. Thus, all compounds exhibit a LUMO of about −3.8 eV and a HOMO value of −6.0 eV with respect to the zero energy level. As expected the differences in electronic properties are negligible for these substitution patterns. This is due to the electronic decoupling of the perylene bisimide core and the imide substituents.[34]

In the following, a detailed study of the structure−property relationship of the different substitution patterns type I−III with respect to thermotropic liquid crystalline behavior is presented. This elucidates the structural requirements for inducing liquid crystalline phases in PBIs.

Thermal and Thermotropic Properties. The thermal stability of the PBIs was analyzed by means of thermogravimetric analysis (TGA) under nitrogen atmosphere. All compounds are stable up to 300 °C (Table 1). Thermotropic behavior of the different derivatives was investigated by a combination of differential scanning calorimetry (DSC) and polarization optical microscopy (POM). Additionally the molecular order within observed mesophases was determined using X-ray diffraction studies (XRD). The TGA data and phase transition temperatures with associated enthalpy values obtained from DSC for all PBIs discussed herein are summarized in Table 1. The DSC data was obtained at a scanning rate of 10 K min^{-1} unless indicated otherwise. The first heating cycles of DSC were neglected to exclude influences of the thermal history of the samples.

(39) Tröster, H. *Dyes Pigm.* **1983**, *4*, 171–177.
(40) Lindner, S. M.; Thelakkat, M. *Macromol. Chem. Phys.* **2006**, *207*, 2084–2092.
(41) Borch, R. F.; Bernstein, M. D.; Durst, H. D. *J. Am. Chem. Soc.* **1971**, *93*, 2897–2904.
(42) Holman, M. W.; Liu, R.; Adams, D. M. *J. Am. Chem. Soc.* **2003**, *125*, 12649–12654.
(43) Zakeeruddin, S. M.; Nazeeruddin, M. K.; Humphry-Baker, R.; Pechy, P.; Quagliotto, P.; Barolo, C.; Viscardi, G.; Graetzel, M. *Langmuir* **2002**, *18*, 952–954.
(44) Kratzat, K.; Finkelmann, H. *Liq. Cryst.* **1993**, *13*, 691–699.
(45) Vacus, J.; Simon, J. *Adv. Mater.* **1995**, *7*, 797–800.
(46) Gürek, A. G.; Ahsen, V.; Heinemann, F.; Zugenmaier, P. *Mol. Cryst. Liq. Cryst. Sci.* **2000**, *338*, 75–97.
(47) Gürek, A. G; Durmus, M; Ahsen, V. *New J. Chem.* **2004**, *28*, 693–699.
(48) Nemoto, H.; Cai, J.; Iwamoto, S.; Yamamoto, Y. *J. Med. Chem.* **1995**, *38*, 1673–1678.
(49) Biron, E.; Otis, F.; Meillon, J.-C.; Robitaille, M.; Lamothe, J.; Van Hove, P.; Cormier, M.-E.; Voyer, N. *Bioorg. Med. Chem.* **2004**, *12*, 1279–1290.
(50) Pommerehne, J.; Vestweber, H.; Guss, W.; Mahrt, R. F.; Bässler, H.; Porsch, M.; Daub, J. *Adv. Mater.* **1995**, *7*, 551–554.

Table 1. Summary of the Thermal Behaviour, Phase Transition[a] Temperatures with Corresponding Transitions Enthalpies and Mesophases of Investigated PBIs **1**−**11** (Obtained from TGA and DSC)

			phase transitions and corresponding enthalpies ΔH (in parentheses) °C/(kJ mol^{-1})	
PBI		T_{dec}[b] °C	2 heating cycle	1 cooling cycle
Type I	**1**	332.9	Cr 133.2 (19.5) → I	I 118.3 (−5.0) → Col_h 110.7 (−11.6) → Cr
	2	296.2	Cr_1 53.8 (6.9) → Cr_2 76.8 (6.6) → I	I 59.3(−6.2) → Cr_2 27.2 (−5.2) → Cr_1
	3	323.5	Cr_1 78.2 (15.8) → Col_h 145.8 (3.5) I	I 141.7 (−3.3) → Col_h 39.8 (−1.8) → Cr_2 21.9 (−3.7) → Cr_1
	4	325.4	Cr 67.8 (24.0) → Col_h 126.9 (3.9) → I	I 121.1 (−3.7) → Col_h
Type II	**5**	329.0	Cr 98.8 (8.5) → I	I 36.3 (−3.7) → Cr
	6	314.6	Cr 77.6 (14.8) → Col_h 154.4 (3.9) → I	I 146.1 (−3.8) → Col_h
	7	339.3	Cr 65.5 (15.0) → Col_h 148.7 (5.9) → I	I 142.0 (−5.7) → Col_h 1.7 (−2.2) → Cr
	8[c]	323.1	Cr 51.0 (10.7) → Col_h 107.7 (3.0) → I	I 105.0 (−2.9) → Col_h 23.5 (−7.6) → Cr
	9	318.7	Cr 54.3 (12.1) → Col_h 111.8 (3.3) → I	I 102.1 (−3.3) → Col_h 1.6 (−3.2) → Cr
Type III	**10**	324.9	Cr 140.1 (10.6) → I	I 129.3 (−10.6) → Cr
	11	334.9	Cr 151.8 (14.3) → I	I 142.0 (−14.0) → Cr

[a] Cr = crystal phase; Col_h = columnar hexagonal mesophase; I = isotropic. [b] Temperature represents 5% weight loss in TGA measurements at a heating rate of 10 K min^{-1} under nitrogen atmosphere. [c] Measured for a heating and cooling rate at 2.0 K min^{-1}.

Transition from an isotropic liquid to crystalline or liquid crystalline phases can be monitored by the evolution of characteristic textures. Additionally, liquid-crystalline phases are anisotropic fluids which in general are optically birefringent. The characteristic textures of liquid crystalline materials result not only from the symmetry-dependent elasticity of the liquid-crystalline phase in combination with defects and surface conditions,[18] but also from thickness and cooling rate of the sample, under investigation. Optical polarization microscopic textures for all the compounds are consistent with the phase transition behavior observed in DSC. All unsymmetrical PBIs carrying one alkyl swallow-tail and one OEG swallow-tail exhibit thermotropic liquid crystalline behavior. In contrast, a reduction of the branched substituents to linear ones results in materials without mesophase bahviour. The evidence of a hexagonal ordered stacking (Col_h) with a high order in the individual columns, was supported by XRD-measurements. The influence of the three different substitution patterns of PBIs under investigation in type I−III are discussed individually in the following paragraphs.

Thermotropic Behavior of Type I, PBIs 1−4. DSC thermogramms of type I PBIs are summarized in Figure 1. In literature there is a controversial discussion, if symmetrically substituted **1** exhibits liquid crystalline behavior.[51−53] It could be shown here, that the symmetrical molecule **1** carrying alkyl substituents exhibits a narrow monotropic hexagonal columnar Col_h mesophase upon cooling from the isotropic melt at 118.3 °C with a phase-width of only 8 °C and crystallizes upon further cooling at 110.7 °C. The evidence of a Col_h ordering was confirmed by polarization microscopy, here typical focal conic textures can be observed under crossed polarizers (Figure 2a). Also a symmetrical analogue **2** with longer alkyl chains (R_1 = $-C_{11}H_{23}$), shows two phase transitions upon heating, and cooling cycle. But here, the first transition in cooling cycle corresponds to a crystallization process that cannot be attributed to a liquid crystalline phase as evidenced by polarization microscopy, where needle-like crystalline aggregates are formed upon annealing the sample at 61 °C (Figure 2b). The second transition at 27 °C corresponds to a crystalline−crystalline transition, but no difference in the optical texture can be observed here. Hence

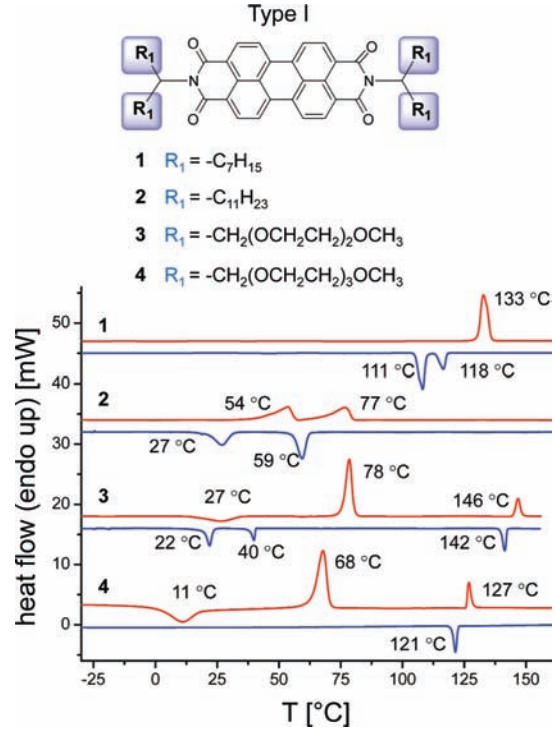

Figure 1. DSC thermograms of symmetrical type I PBIs **1**, **2**, **3** and **4** showing the second heating and first cooling cycle at a heating rate of 10 K min^{-1} with respective transition temperatures (°C). Red curves represent the second heating cycle and blue curves represent the first cooling cycle.

a simple increase in substituent length does not help to increase the mesophase temperature-width of compound **1**, but even results in crystalline behavior.

On the other hand, a change from alkyl swallow-tail to OEG swallow-tail substituents in case of PBIs **3** and **4**, results in liquid crystalline behavior. This can be attributed to the higher conformational freedom of the C−O bond compared to C−C bond allowing for a better space filling around the discotic mesogen. In contrast to symmetrical dialkyl swallow-tail PBI **1**, the compounds **3** and **4** have a much broader liquid crystalline phase which is not monotropic. Additionally, the length of the OEG swallow-tail substituent influences the clearing temperature of PBIs (**3**: T_{iso} = 145.8 °C; **4**: T_{iso} = 126.9 °C). As expected compound **4** with longer OEG substituent exhibits a lower clearing temperature, whereas the enthalpy $\Delta H_{Col_h \rightarrow iso}$ remains almost the same. The transition temperature from the crystalline

(51) Pisula, W.; Kastler, M.; Wasserfallen, D.; Robertson, J. W. F.; Nolde, F.; Kohl, C.; Muellen, K. *Angew. Chem., Int. Ed.* **2006**, *45*, 819–823.
(52) Marcon, V.; Kirkpatrick, J.; Pisula, W.; Andrienko, D. *Phys. Status Solidi* **2008**, *245*, 820–824.
(53) Hansen, M. R.; Graf, R.; Sekharan, S.; Sebastiani, D. *J. Am. Chem. Soc.* **2009**, *131*, 5251–5256.

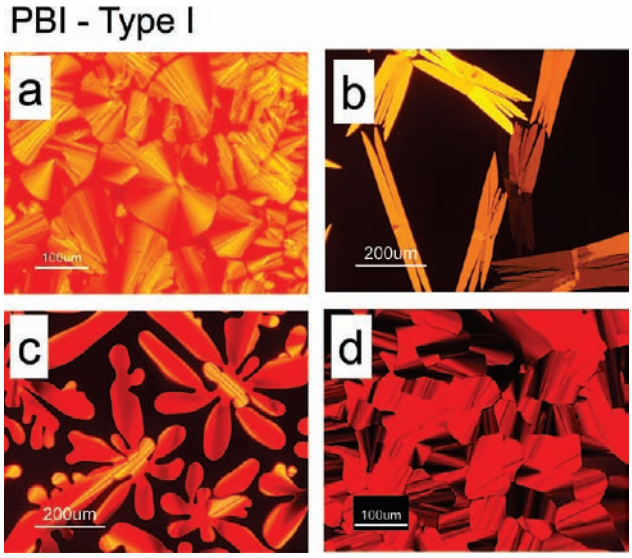

Figure 2. Optical microscopic images of textures of PBIs type I (under crossed polarizers) of (a) **1** annealed in the mesophase at 118 °C showing typical focal conic texture of Col_h phase, (b) long needle-like crystals of **2** at 61.2 °C, (c) **3** in mesophase at 144 °C showing dendritic growth aggregates of Col_h phase and (d) **4** at 142 °C showing fan-shaped focal conic textures. The textures were obtained upon cooling the sample from the isotropic phase and annealing at the respective temperatures slightly above phase-transition temperature.

phase to the liquid crystalline phase Cr → Col_h is shifted only slightly from 78.2 °C for **3** to 67.8 °C for **4**. But here the enthalpy of the melting process to the liquid crystalline phase is with 24.0 kJ mol^{-1} for **4** much higher than 15.8 kJ mol^{-1} for **3**. In the heating cycle, the LC phase-width is 68 °C for **3** and 59 °C for **4**, and in the cooling cycle the LC phase-width for **3** is with 102 °C larger, due to supercooling of crystallization. For PBI **4**, the crystallization transition upon cooling cycle could not be detected in DSC (10 K min^{-1}), but here XRD-measurements at RT showed typical multiple crystalline reflections. Also the texture observed in POM was not shearable at room temperature anymore. Transition from an isotropic liquid to columnar hexagonal mesophase (Col_h) for both **3** and **4** was observed in POM as indicated by the formation of typical dendritic growth aggregates or fan-shaped focal conic textures upon cooling the sample from the isotropic melt under crossed polarizers (Figure 2c, d). The straight linear defects observed in several textures are also characteristic for an ordered columnar mesophase.[18,19] These textures are highly shearable in the mesophase range and no crystallization was observed upon cooling, only the viscosity of the LC-phase increases upon cooling to room temperature. For **3** an additional crystalline−crystalline transition at 22 °C can be observed upon cooling the sample in DSC. For this transition no textural changes could be observed in polarization microscopy and X-ray scattering experiments could not be performed at temperatures below room temperature, but the XRD-pattern at room temperature showed multiple reflections typical for a crystalline material. Due to the high viscosity of the mesophase the crystallization is supercooled in DSC (even at slow scanning rates) and partial recrystallization occurs for both materials upon heating the sample again. In short, a simple increase in the alkyl substituent length does not result in liquid crystalline behavior, but a change in the nature of the substituent from alkyl to OEG helps to induce liquid crystallinity in the case of symmetrically substituted swallow-tail PBI of type I.

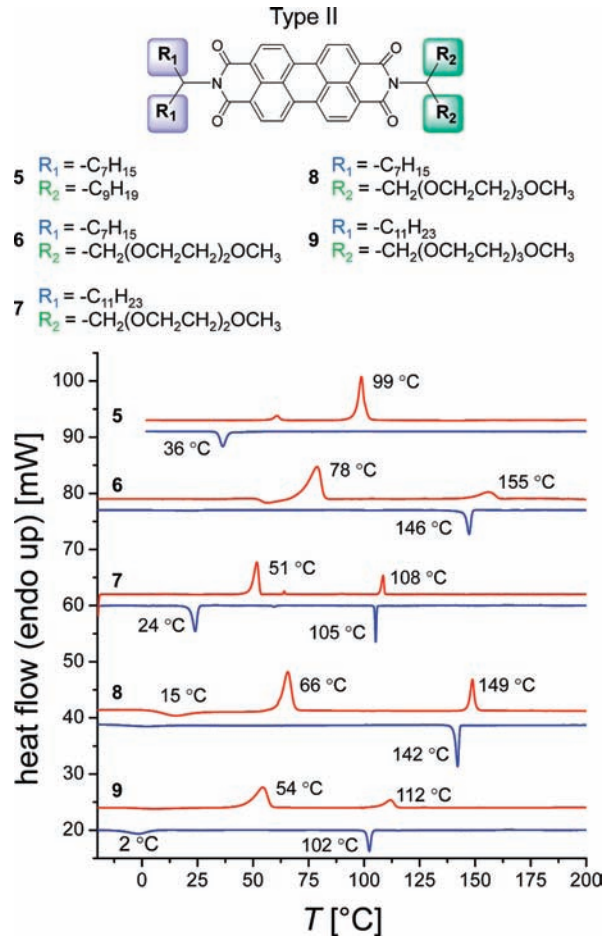

Figure 3. DSC thermograms of unsymmetrical type II PBIs **5**, **6**, **8**, **9** (10 K min^{-1}) and **7** (2 K min^{-1}) showing the second heating and first cooling cycle with respective transition temperatures (°C). Red curves show the second heating cycle and blue curves represent the first cooling cycle.

Thermotropic Behavior of Type II, PBIs 5−9. DSC thermograms of type II PBIs are summarized in Figure 3. The unsymmetrical compound **5** carrying two different alkyl swallow-tail substituents remains crystalline. Also a comparison of **1**, **2** and **5** clearly shows that the LC-phase observed in **1** could not be broadened in **2** or **5**, both by extending the length of substituents or by introducing unsymmetrical substitution. However, the unsymmetrical PBIs with one OEG swallow-tail substituent and one alkyl swallow-tail substituent (**6**−**9**) resulted in thermotropic liquid crystalline derivatives. Moreover, in the unsymmetrical molecules **6**−**9**, an increase in alkyl chain length has only a marginal influence in decreasing the clearing temperature, whereas a corresponding increase in OEG length decreases the clearing temperature considerably. Thus for instance **6** with two oxyethylene repeating units clears at 154.9 °C and **7** carrying three oxyethylene repeating units shows a clearing temperature of 108.5 °C; a difference of 46 °C. Similarly compound **8** with a shorter OEG substituent clears at 148.4 °C compared to **9** carrying a longer OEG substituent at 111.8 °C, the difference being 37 °C. Thus the clearing temperature can be tuned by appropriate substituent length. Generally the transition from Col_h phase to crystalline phase is strongly supercooled here and recrystallization could be observed upon heating cycles. The crystallization processes can be observed more clearly at a heating rate of 2 K min^{-1}. The effect of supercooling, for example observed in **6**, **8** or **9**, allows

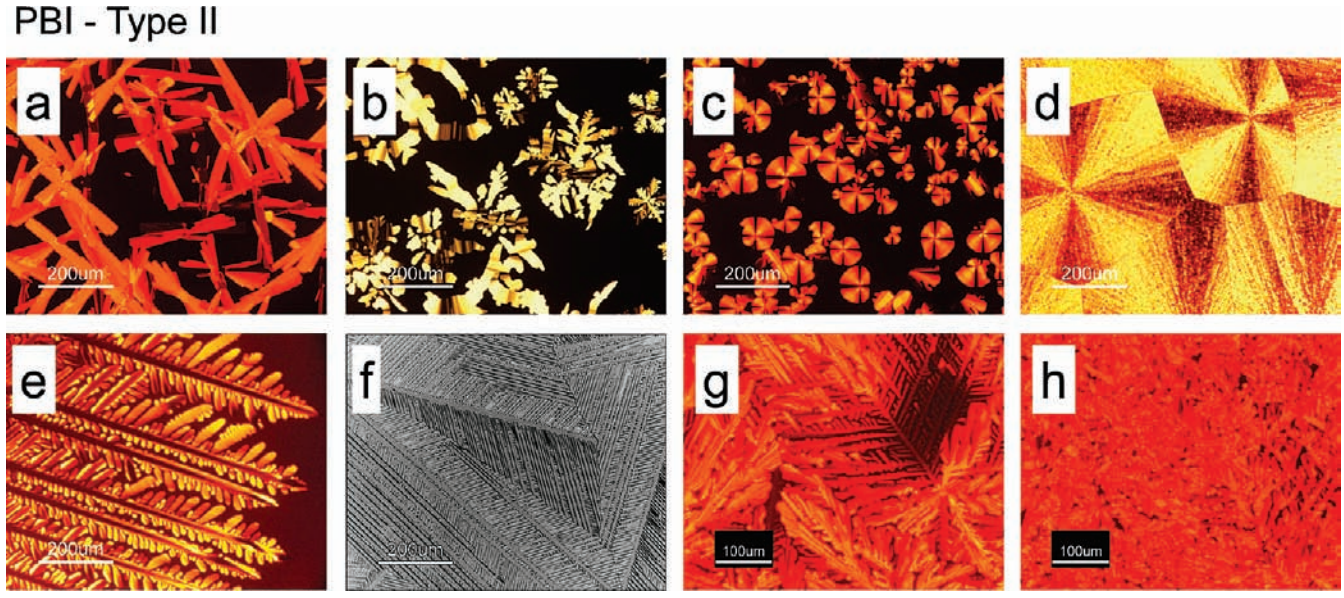

Figure 4. Optical microscopic images of textures of PBIs **5**−**9** (under crossed polarizers) of (a) crystals of **5** fromed upon annealing at 63 °C, (b) texture of **6** at 153 °C showing dendritic growth snowflake-like aggregates of Col_h phase but also ribbons with straight linear defects that are characteristic for ordered columnar mesophases, (c) **7** at 108 °C showing spherulitic texture with maltese crosses of Col_h phase, (d) **8** at 141 °C showing large spherulitic texture of Col_h phase formed upon fast cooling from isotropic melt and (e) **8** large dendritic growth aggregates of Col_h phase formed upon annealing at 149 °C. (f) **8** annealed at 149 °C at different film region showing dendritic growth agreggates, here a $\lambda/4$ plate is utilized to visualize partial homeotropic ordering, (g) PBI **9** annealed in the mesophase at 108 °C showing typical dendritic-growth aggregates of the Col_h phase and (h) **9** sheared-film at same film position. The textures were obtained upon cooling the sample from the isotropic phase and annealing at the respective temperatures slightly above phase-transition temperature.

for freezing in the mesophase. This finding is of great relevance when these PBIs are employed in electronic devices.

For these PBIs **6**−**9** the evidence of Col_h liquid crystalline behavior was further confirmed by POM (Figure 4). The unsymmetrical type II PBIs **6**−**9** carrying one OEG swallow-tail substituent show characteristic Col_h textures. Figure 4a depicts the crystalline texture of PBI **5** which does not exhibit any liquid crystalline behavior. In contrast, for PBI **6**, large snowflake-like dendritic-growth aggregates of Col_h phase as well as ribbons with straight linear defects that are characteristic for ordered columnar mesophases can be observed at 153 °C (Figure 4b). Figure 4c represents the texture of **7** at 108 °C showing spherulitic textures with maltese crosses, also typical for a Col_h ordering. Figure 4d shows compound **8** at 141 °C showing large spherulitic textures of Col_h phase formed upon fast cooling from isotropic melt, whereas extremely large dendritic aggregates of the Col_h phase are formed upon annealing **8** at 149 °C (Figure 4e). Additionally domains with homeotropic alignment can be observed for **8** if a $\lambda/4$-plate is employed in front of the analyzer for the slowly cooled sample (Figure 4f). This indicates an ordering parallel to the substrate surface (homeotropic alignment) at low cooling velocities. Figure 4g shows the texture of **9** annealed in the mesophase at 108 °C displaying typical dendritic aggregates of Col_h phase and Figure 4h represents the texture upon shearing the sample at the same film position, illustrating the high viscosity of these systems.

It is highly interesting to compare PBIs **5** and **6**, both bearing an identical number of side chain atoms. The only difference here lies in the flexibility of the respective substituents. For both PBIs, R_1 is $-C_7H_{15}$, but R_2 differs in flexibility. In **5** an alkyl swallow-tail substituent is used, in contrast to an OEG swallow-tail substituent in **6**. It can be observed that **5** melts from the crystalline state into the isotropic phase at 99 °C and the respective crystallization upon cooling is strongly supercooled and occurs at 36 °C (Figure 3). Also the crystallization process of **5** upon annealing at 63 °C can be observed in POM (Figure 4a). On the other hand PBI **6** exhibits Col_h mesophase which can be attributed to the presence of OEG substituent. Thus, the introduction of two different alkyl swallow-tail substituents with different spatial demands does not result in liquid crystalline behavior. In contrast, in **6**, employing a combination of alkyl swallow-tail substituents with OEG swallow-tail substituents, broad liquid crystalline mesophases can be observed (77 °C mesophase window in the heating cycle). In short, the comparison of **5** and **6** clearly indicates the ability of ether substituents to suppress the crystallization tendency of the perylene bisimide moiety.

Thermotropic Behaviour of Type III, PBIs 10 and 11. A reduction of the size of the *N*-substituents is of fundamental interest in designing PBI semiconductors for device applications in order to keep the content of the electronically active perylene chromophore high. To this end, one of the swallow-tail substituents was replaced with a linear one in type III compounds. Thus unsymmetrical PBIs **10** and **11** with one swallow-tail and one linear substituent were synthesized. Both **10** and **11** are crystalline materials as can be seen from DSC-thermograms (Figure 5) and POM textures (Figure 6a, b). PBI **10** melts at 140 °C whereas **11** shows a melting peak at 152 °C. Both compounds recrystallize on cooling and do not exhibit any supercooling effect. The absence of any mesophase indicates that the linear substituents are spatially less demanding and may not be able to fill the space sufficiently around the columnar stacked PBI molecules.

X-Ray Diffraction Experiments on Liquid Crystalline PBIs. Additionally X-ray diffraction experiments were carried out to clearly elucidate the order parameters and to confirm the nature of the mesophases of the liquid crystalline PBIs **1**, **3**, **4**, **6**, **7**, **8** and **9** unequivocally. This also helps to understand the

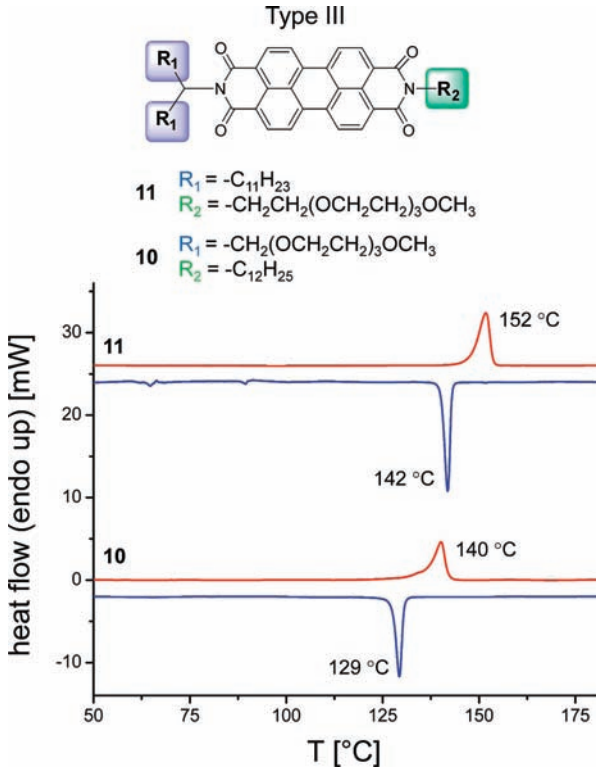

Figure 5. DSC thermograms of unsymmetrical type III PBIs, **10** and **11**, showing the second heating and first cooling cycle at a heating rate of 10 K min^{-1} with respective transition temperatures (°C). Red curves show the second heating cycle and blue curves represent the first cooling cycle.

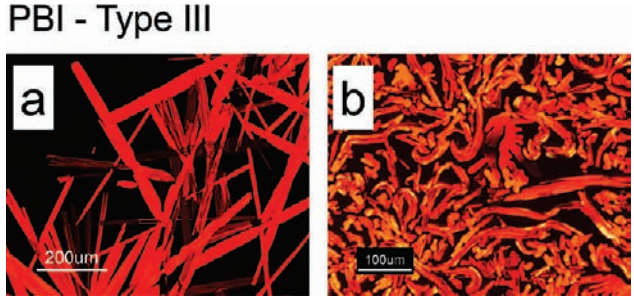

Figure 6. Optical microscopic images of crystalline of type III PBIs (under crossed polarizers). (a) Very long crystals of **11** formed upon annealing at 145 °C and (b) crystals of **10** formed upon annealing at 135 °C. The textures were obtained upon cooling the sample from the isotropic phase and annealing at the respective temperatures slightly above phase-transition temperature.

effect of the different substituents on hexagonal lattice parameters. Figure 7 presents the geometry and packing paramaters for the columnar hexagonal liquid crystalline mesophase (Col_h).[18] Packing parameters for PBIs under investigation as determined from X-ray diffraction experiments are summarized in Table 2.

Symmetrical type I PBIs **1**, **3** and **4** show the d_{100} and d_{110} reflections displaying a columnar hexagonal mesophase with the characteristic perylene-perylene stacking-distance of c = 3.4−3.5 Å (from d_{001} reflection at about 25.5°) in the columns (Figure 8). Additionally, the sharp d_{001} reflexes at approximately 25.5° for all LC compounds are typical for a high order in the intracolumnar packing of the discotic molecules. For **1**, the d_{100} and d_{200} reflections can be observed. The diffuse halo at bigger angles (>10°) arises from the liquid-like *N*-substituents. As

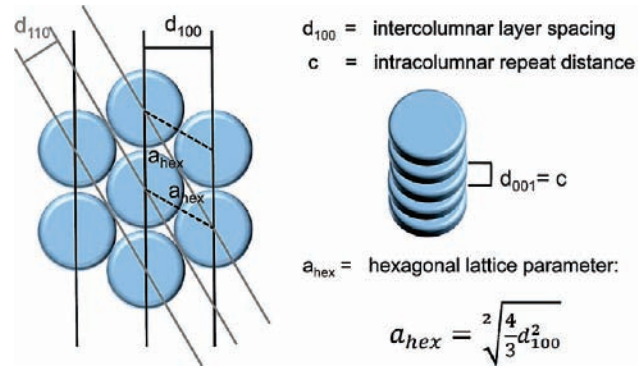

Figure 7. Schematic representation of discotic columnar hexagonal packing parameters in liquid crystalline mesophases. Intercolumnar layer spacing d_{100}, hexagonal lattice parameter a_{hex} and intracolumnar repeat distance c (d_{001}) for discotic molecules. More geometric considerations result in the characteristic ratios of $1:\frac{1}{\sqrt{3}}:\frac{1}{\sqrt{4}}:\frac{1}{\sqrt{7}}:\frac{1}{\sqrt{9}}:\frac{1}{\sqrt{12}}:\frac{1}{\sqrt{13}}$ for the d spacings of the (100), (110), (200), (210), (300), (220), and (310) reflections of a hexagonal lattice in the small-angle regime.

Table 2. Hexagonal Lattice Parameters: Intercolumnar Layer Spacing d_{100} [Å], Hexagonal Lattice Parameter a_{hex} [Å] and Intracolumnar Repeat Distance c [Å] for PBIs **1**, **3**, **4**, **6**, **7**, **8** and **9** in the Liquid Crystalline Mesophase, as Determined from Temperature Dependent X-Ray Diffraction Experiments

PBI	R_1/R_2	*T* [°C]	phase	d_{100} [Å]	a_{hex}[a] [Å]	c [Å]
1	$R_1 = R_2 = C_7H_{15}$	120	Col_h	18.02	20.81	3.51
3	$R_1 = R_2 = CH_2(OCH_2CH_2)_2OMe$	100	Col_h	18.02	20.81	3.48
4	$R_1 = R_2 = CH_2(OCH_2CH_2)_3OMe$	80	Col_h	19.89	22.97	3.48
6	$R_1 = C_7H_{15}$, $R_2 = CH_2(OCH_2CH_2)_2OMe$	120	Col_h	18.39	21.23	3.48
7	$R_1 = C_7H_{15}$, $R_2 = CH_2(OCH_2CH_2)_3OMe$	120	Col_h	19.19	22.16	3.49
8	$R_1 = C_{11}H_{23}$, $R_2 = CH_2(OCH_2CH_2)_2OMe$	90	Col_h	19.89	22.97	3.46
9	$R_1 = C_{11}H_{23}$, $R_2 = CH_2(OCH_2CH_2)_3OMe$	90	Col_h	20.73	23.94	3.47

[a] Hexagonal lattice parameter $a_{hex} = \sqrt[2]{(4/3\ d_{100}^2)}$.

expected, **4** with the larger OEG-substituent also has the biggest unit cell a_{hex} = 22.97 Å. Interestingly PBI **1** carrying only alkyl substituents has the same hexagonal packing parameter a_{hex} = 20.81 Å as PBI **3** with a comparatively larger OEG *N*-substituent. This fact also implies a higher conformational freedom in the packing behavior of the OEG-substituents compared to alkyl substituents.

Also for the unsymmetrically substituted type II PBIs **6**, **7**, **8** and **9**, the diffractogramm (Figure 9) exhibits the typical liquid crystalline columnar hexagonal Col_h reflections d_{100} and d_{110}. The differences in d_{100} are about 0.8 Å on changing the oxyethylene repeating units from two to three in compounds **6** vs **7** as well as **8** vs **9**. On the other hand, a change of about 1.5 Å in d_{100} spacing was observed for compounds **6** vs **8** as well as **7** vs **9**, in which the alkyl substituent length was varied from $R_1 = -C_7H_{15}$ to $-C_{11}H_{23}$ respectively, maintaining the OEG length the same. Also on comparison, compound **4** carrying only OEG swallow-tail substituents exhibits a smaller d_{100} value of 19.89 Å than **9** with alkyl and OEG substituents with comparable length (d_{100} = 20.73 Å). This shows that the ether side chains pack more tightly than alkyl substituents due to higher conformational freedom of the C−O bond in OEG.

The unsymmetrical type III PBIs **10** and **11** with one linear side chain and one swallowtail side chain show several crystalline reflections in XRD, typical for polycrystalline materials.

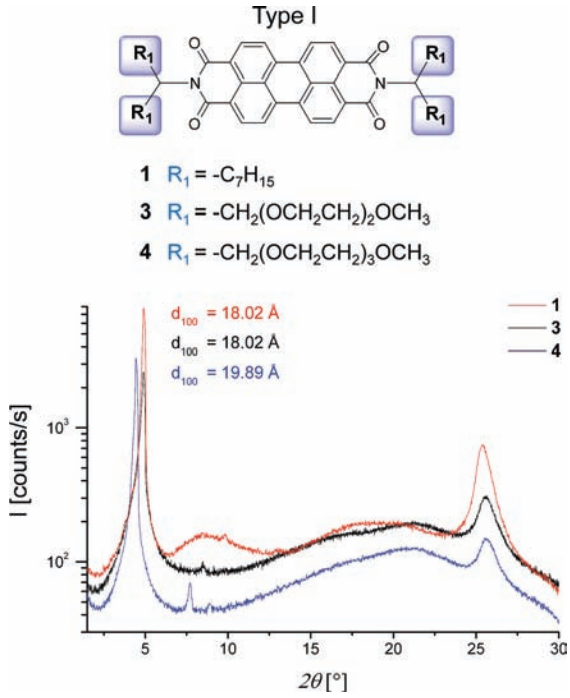

Figure 8. X-ray diffraction patterns of Col_h perylene bisimides **1** (at 120 °C), **3** (at 100 °C) and **4** (at 80 °C) measured in the Col_h mesophase.

Conclusion

Several symmetrically and unsymmetrically *N*-substituted perylene bisimides have been successfully synthesized by two different synthetic strategies. The substituents used involved swallow-tail and linear alkyl- or oligooxyethylene (OEG) substituents. The focus of investigation was directed toward designing tailor-made liquid crystalline PBIs and to elucidate a structure−property relationship with respect to thermotropic behavior in *N*-substituted derivatives of PBIs. To this end, only *N*-substitution was considered and bay substitution was avoided to keep the optical and electronical properties similar. Thermotropic behavior was examined by DSC, POM and XRD measurements in the mesophase temperature range. Several PBIs exhibiting columnar hexagonal liquid crystalline Col_h behavior with broad LC temperature window were obtained by this approach. It could be shown that OEG swallow-tail substituents efficiently support Col_h behavior and that both *N*-substituents have to be branched in nature. A reduction to linear *N*-substituents resulted in strongly crystalline behavior. By an unsymmetrical substitution pattern, the melting point to the liquid crystalline phase as well as clearing temperature could be controlled very efficiently. Upon cooling the LC phase, the crystallization process of these PBIs is strongly supercooled. Thus, these novel liquid crystalline PBIs are highly promising candidates to be applied in organic electronics like field-effect transistors or photovoltaic devices. Our current investigations toward devices deal with substrate/molecule interaction and orientation of these molecules on alignment layers deposited on device substrates. Preliminary results indicate uniaxial edge-on to the surface orientation of molecules, which is ideal for OFETs. The detailed device results will be published later.

Experimental Section

Materials and Methods. The starting materials, perylenetetracarboxylic acid dianhydride PTCDA, pentadecane-8-one, tricosan-12-one, 1-bromononane, diethylenglycol monomethyl ether, triethylenglycol monomethyl ether, tetraethyleneglycol monomethyl ether and solvents, were purchased from Merck, Aldrich, Fluka or TCI and used without any further purification. Solvents used for precipitation and column chromatography were distilled under normal atmosphere. For the synthesis of perylene intermediates **12a**,**b**[35,54] and **14a**−**c**,[36] see Supporting Information. All swallow-tail and linear bromides[43,49] or amines[41,42,44−48] respectively were synthesized according to published procedures.

^{1}H- and ^{13}C NMR spectra were recorded on a Bruker AC 250 spectrometer (250 MHz). Chemical shifts are reported in ppm at room temperature using $CDCl_3$ as solvent and tetramethylsilane as internal standard unless indicated otherwise. Abbreviations used for splitting patterns are *s* = singlet, *d* = dublett, *t* = triplet, qui = quintet, *m* = multiplet. Gel permeation chromatography (GPC) was performed on a Waters size exclusion chromatography system for oligomers (analytical columns: cross-linked polystyrene gel, length 2 × 60 cm, width 0.8 cm, particle size 5 μm, pore size 100 Å, eluent THF (0.5 mL min^{-1}, 80 bar), and polystyrene calibration). IR spectroscopy was carried out with a BioRad Digilab FTS-40 (FT-IR) in the range of 400−4000 cm^{-1}. Mass spectroscopic data were obtained from a FINNIGAN MAT 8500 instrument. Microanalyses were carried out with a PERKIN-ELMER 2400 CHN elemental analyzer. The thermal degradation of PBI derivatives was studied using a Mettler Toledo TGA/SDTA 851^e with a heating rate of 10 K min^{-1} under N_2 atmosphere. Differential scanning calorimetry (DSC) was carried out with a Perkin-Elmer Diamond DSC with a heating rate of 10 K min^{-1} unless otherwise indicated under N_2-atmosphere. The instrument was calibrated with indium

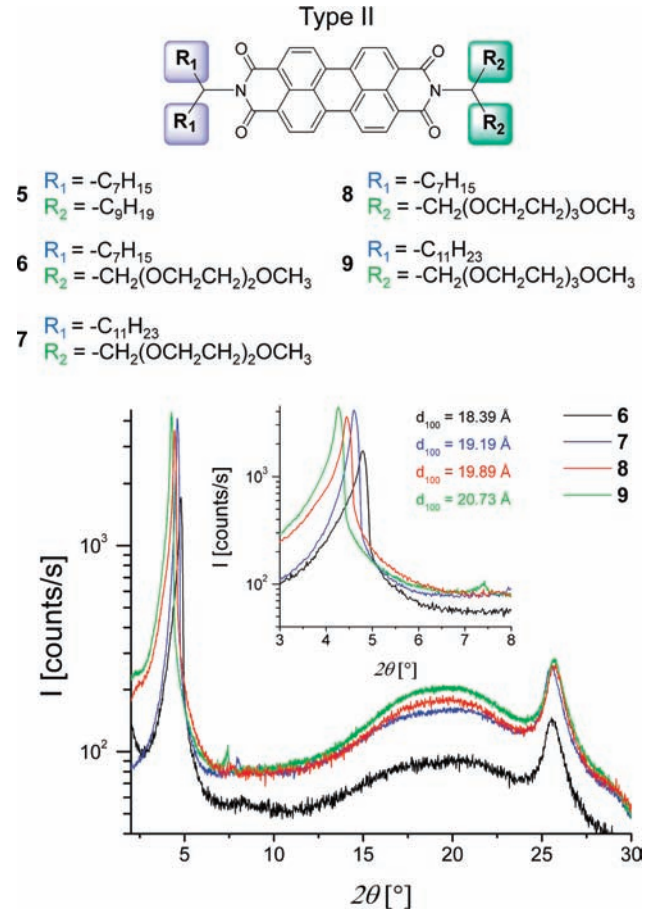

Figure 9. X-ray diffraction patterns of perylene bisimides **6** (at 120 °C), **7** (at 120 °C), **8** (at 90 °C) and **9** (at 90 °C) measured in the Col_h mesophase. (Inset) d_{100} intercolumnar reflections with respective repeat distances.

(54) Wescott, L. D.; Mattern, D. L. *J. Org. Chem.* **2003**, *68*, 10058–10066.

standards before measurements. Phase transitions were also examined by a polarization optical microscop (POM) Nikon Diaphot 300 with a Mettler FP 90 temperature-controlled hot stage. X-ray diffraction measurements were performed on a Huber Guinier Diffraktometer 6000 equipped with a Huber quartz monochromator 611 with Cu−$K_{\alpha1}$: 1.54051 Å. For cyclic voltammetry (CV) experiments, a conventional three-electrode assembly using a Ag/$AgNO_3$ reference electrode was used. CH_2Cl_2 containing 0.1 M Bu_4NPF_6 was used as solvent. All measurements were carried out under N_2-atmosphere at a scan rate of 0.05 V s^{-1} at 25 °C and all redox potentials were calibrated to ferrocene/ferrocenium couple (Fc/Fc^+).

General Procedure for the Preparation of Symmetrical *N*,*N*′-Di(1-alkyl swallow-tail)-perylene-3,4,9,10-tetracarboxylic Bisimides 1 and 2.[35,54] A mixture of perylene-3,4,9,10-tetracarboxylic dianhydride PTCDA (1.0 mmol), $Zn(OAc)_2$ (0.75 mmol), imidazole (4.0 g) and the respective alkyl swallow-tail amine (3.0 mmol) was vigorously stirred at 160 °C for 2 h. After cooling to r.t., the mixture was dissolved in minimum amount of THF and precipitated in 300 mL 2N HCl/MeOH 2:1 *v/v*. The precipitate was collected by filtration, washed with H_2O followed by MeOH and dried at 80 °C in vacuum. The crude product was further purified by column chromatography.

***N*,*N*′-Di(1-octylheptyl)-perylene-3,4,9,10-tetracarboxylic Bisimide 1.** Perylene-3,4,9,10-tetracarboxylic dianhydride (1.96 g, 5.0 mmol) and 8-octylheptylamine (3.41 g, 15.0 mmol) were allowed to react according to the above general procedure. The crude product was further purified by silica flash-column chromatography with n-hexane/$CHCl_3$ 2:1 *v/v*. The final product was freeze-dried from benzene and was obtained as a red solid (2.68 g, 66.1%). Mp 135.5 °C. Calcd for $C_{54}H_{70}N_2O_4$: C 79.96, H 8.70, N 3.45. Found: C 79.84, H 8.59, N 3.32. EI-MS (70 eV): *m/z* 811.0 [M^+, 70.78%]. IR (ATR): ν = 2952 m, 2922 m, 2853 m, 1697 s, 1654 s, 1593 s, 1578 m, 1505 w, 1460 m, 1433 m, 1404 m, 1335 s, 1251 m, 1207 m, 1172 m, 1123 w, 1108 w, 962 w, 850 w, 809 m, 795 w, 745 m, 723 cm^{-1} m. ^{1}H NMR (250 MHz, $CDCl_3$, 298K): δ = 0.82 (t, *J* = 6.8 Hz, 12*H*, $4CH_3$), 1.12−1.41 (m, 40*H*, $20CH_2$), 1.77−1.96 (m, 4*H*, $2\alpha CH_2$), 2.15−2.36 (m, 4*H*, $2\alpha CH_2$), 5.10−5.27 (m, 2*H*, N−CH), 8.52−8.76 (m, 8*H*, 8ArH) ppm. ^{13}C NMR (62.5 MHz, $CDCl_3$, 298K): δ = 14.40 (4C, CH_3), 22.95, 27.32, 29.56, 29.85, 32.14, 32.71 (24C, CH_2), 55.11 (2C, N−CH), 123.35, 123.54, 124.28, 131.46, 132.23, 126.77, 129.93, 134.83 (20C, C_{Ar}), 163.90, 164.99 (4C, CONR) ppm.

***N*,*N*′-Di(1-dodecylundecyl)-perylene-3,4,9,10-tetracarboxylic Bisimide 2.** Perylene-3,4,9,10-tetracarboxylic dianhydride (3.92 g, 10 mmol) and 12-dodecylundecylamine (10.19 g, 30.0 mmol) were allowed to react according to the general procedure. The crude product was further purified by silica flash-column chromatography with $CHCl_3$. The final product was freeze-dried from benzene and was obtained as an orange solid (9.76 g, 94.3%). Mp 76.8 °C. Calcd for $C_{70}H_{102}N_2O_4$: C 81.19, H 9.93, N 2.71. Found C 80.93, H 9.56, N 2.47. EI-MS (70 eV): *m/z* 1033.8 [M^+, 76.14%]. IR (ATR): ν = 2952 m, 2919 s, 2849 s, 1694 s, 1650 s, 1592 s, 1577 m, 1507 w, 1466 m, 1434 w, 1405 m, 1335 s, 1273 w, 1252 s, 1211 w, 1194 w, 1175 w, 1156 w, 1125 w, 1100 w, 959 w, 866 w, 856 w, 844 w, 813 s, 796 w, 773 w, 750 s, 721 m cm^{-1}. ^{1}H NMR (250 MHz, $CDCl_3$, 298K): δ = 0.83 (t, *J* = 6.8 Hz, 12*H*, $4CH_3$), 1.01−1.44 (m, 72*H*, $36CH_2$), 1.76−1.96 (m, 4*H*, $2\alpha CH_2$), 2.15−2.34 (m, 4*H*, $2\alpha CH_2$), 5.09−5.26 (m, 2*H*, N−CH), 8.52−8.76 (m, 8*H*, 8ArH) ppm. ^{13}C NMR (62.5 MHz, $CDCl_3$, 298K): δ = 14.43 (4C, CH_3), 23.00, 27.30, 29.66, 29.88, 29.92, 29.94, 29.95, 32.24, 32.70 (36C, CH_2), 55.11 (2C, N−CH), 123.32, 131.45, 132.21, 123.54, 124.30, 126.76, 129.92, 134.80 (20C, C_{Ar}), 163.90, 164.97 (4C, CONR) ppm.

General Procedure for the Preparation of Symmetrical *N*,*N*′-Di(1-OEG swallow-tail)-perylene-3,4,9,10-tetracarboxylic Bisimides 3 and 4:[24] A mixture of perylene-3,4,9,10-tetracarboxylic dianhydride PTCDA (10.0 mmol), $Zn(OAc)_2$ (7.5 mmol) in dry pyridine (75.0 mL) and the respective OEG swallow-tail amine (27.0 mmol) was stirred at 140 °C for 48 h. The resulting burgundy colored mixture was cooled, diluted with methylene chloride, and filtered through Celite to remove excess dianhydride. The filtrate was dried over $MgSO_4$ and concentrated under reduced pressure. The crude product was further purified by flash column chromatography.

***N*,*N*′-Di(2-(1,3-bis(2-(2-(2-methoxyl)ethoxyl)ethoxyl)propyl))-perylene-3,4,9,10-tetracarboxylic Bisimide 3.** Perylene-3,4,9,10-tetracarboxylic dianhydride (5.12 g, 13.03 mmol) and 1,3-bis(2-(2-methoxyethoxy)ethoxy) propane-2-amine (10.34 g, 35.2 mmol) were allowed to react according to the general procedure. The crude product was further purified by silica flash-column chromatography with $CHCl_3$ and then $CHCl_3$/MeOH 98:2 *v/v*. The final product was freeze-dried from benzene and was obtained as a red solid (10.7 g, 81.6%). Mp 145.8 °C. Calcd for $C_{50}H_{62}N_2O_{16}$: C 63.41, H 6.60, N 2.96. Found C 63.19, H 6.63, N 2.85. EI-MS (70 eV): *m/z* 946.7 [M^+, 10.70%]. IR (ATR): ν = 2984 w, 2920 m, 2870 m, 2825 w, 1695 s, 1653 s, 1593 s, 1575 m, 1508 w, 1459 w, 1435 w, 1359 m, 1341 s, 1305 w, 1284 w, 1253 m, 1196 w, 1182 w, 1092 s, 1052 m, 1026 m, 962 m, 947 m, 850 m, 810 s, 796 m, 745 s, 711 w cm^{-1}. ^{1}H NMR (250 MHz, $CDCl_3$, 298K): δ = 3.27 (s, 12*H*, $4OCH_3$−OEG), 3.38−3.45 (m, 8*H*, $4OCH_2$−OEG), 3.52−3.78 (m, 24*H*, $12OCH_2$−OEG) 3.98 (dd, *J* = 10.6 Hz, *J* = 5.9 Hz, 4*H*, 2αOCH2-OEG), 4.19 (dd, *J* = 10.6 Hz, *J* = 7.8 Hz, 4*H*, 2αOCH2-OPEG), 5.63−5.79 (m, 2*H*, 2N−CH-OEG), 8.46−8.72 (m, 8*H*, 8ArH in perylene ring) ppm. ^{13}C NMR (62.5 MHz, $CDCl_3$, 298K): δ = 52.51 (2C, N−CH), 59.28 (4C, OCH_3), 69.66, 70.70, 70.80, 70.85, 72.17 (10C, OCH_2), 123.20, 123.63, 126.31, 129.57, 131.64, 134.50 (20C, C_{Ar}), 164.03 (4C, CONR) ppm.

***N*,*N*′-Di(2-(1,3-bis(2-(2-(2-methoxyl)ethoxyl)ethoxyl)ethoxyl)-propyl))-perylene-3,4,9,10-tetracarboxylic Bisimide 4.** Perylene-3,4,9,10-tetracarboxylic dianhydride (785 mg, 2.0 mmol) and 1,3-bis(2-(2-(2-methoxyethoxy)ethoxy)ethoxy)propane-2-amine (2.07 g, 5.4 mmol) were allowed to react according to the general procedure. The crude product was further purified by silica flash-column chromatography with $CHCl_3$ and then $CHCl_3$/MeOH 98:2 *v/v*. The final product was freeze-dried from benzene and was obtained as a red solid (1.79 g, 79.6%). Mp 126.9 °C. Calcd for $C_{58}H_{78}N_2O_{20}$: C 62.02, H 7.00, N 2.49. Found: C 61.58, H 6.69, N 2.28. IR (ATR): ν = 2976 w, 2912 w, 2868 m, 2821 w, 1694 s, 1653 s, 1593 m, 1575 m, 1448 w, 1435 w, 1404 m, 1355 m, 1343 s, 1307 w, 1250 m, 1197 w, 1181 w, 1135 m, 1098 s, 1052 m, 1026 m, 967, m, 875 w, 858 m, 809 s, 797 w, 745 s, 711 w cm^{-1}. ^{1}H NMR (250 MHz, $CDCl_3$, 298K): δ (ppm) = 3.32 (s, 12*H*, $4OCH_3$−OEG), 3.42−3.78 (m, 48*H*, $12OCH_2$−PEG), 3.97 (dd, *J* = 10.6 Hz, *J* = 5.8 Hz, 4*H*, 2αOCH2-OEG), 4.20 (dd, *J* = 10.6 Hz, *J* = 7.8 Hz, 4*H*, 2αOCH2-OEG), 5.64−5.76 (m, 2*H*, 2N−CH-OEG), 8.41−8.60 (m, 8*H*, 8ArH). ^{13}C NMR (62.5 MHz, $CDCl_3$, 298K): δ = 52.46 (2C, N−CH), 59.32 (4C, OCH_3), 69.66, 70.67, 70.79, 70.82, 70.87, 72.21 (28C, OCH_2), 123.35, 123.74, 126.56, 129.77, 131.79, 134.74 (20C, C_{Ar}), 164.13 (4C, CONR).

General Procedure for the Preparation of Unsymmetrical *N*-(1-Alkyl swallow-tail)-*N*′-(1-OEG swallow-tail)-perylene-3,4,9,10-tetracarboxylic Bisimides 6, 7, 8, and 9 via Condensation Reaction. A mixture of the respective *N*-(1-alkyl swallow-tail)-perylene-3,4,9,10-tetracarboxylic-3,4-anhydride-9,10-imide (1.0 mmol), $Zn(OAc)_2$ (1.5 mmol) in dry DMAc (6.0 mL) and the respective amine (1.8 mmol) was stirred in a microwave pressure reactor for 20 min at 160 °C and 200 W. After cooling to r.t. the mixture was dissolved in minimum amount of THF and precipitated in 300 mL 2N HCl/MeOH 2:1 *v/v*. After standing overnight, the precipitate was collected by filtration, washed with H_2O, then MeOH and dried at 60 °C in vacuum. The crude product was further purified by column chromatography on silica flash-gel (see respective compound for details).

***N*-(1-octylheptyl)-*N*′-(2-(1,3-bis(2-(2-(2-methoxyl)ethoxyl)ethoxyl)-propyl))-perylene-3,4,9,10-tetracarboxylic Bisimide 6.** *N*-(1-octylheptyl)-perylene-3,4,9,10-tetracarboxylic-3,4-anhydride-9,10-imide **12a** (602 mg, 1 mmol) and 1,3-bis(2-(2-methoxyethoxy)ethoxy)

propane-2-amine (532 mg, 1.8 mmol) were allowed to react according to the general procedure. The crude product was further purified by silica flash-column chromatography with $CHCl_3$/AcOH 10:1 *v/v* to elute impurities and then $CHCl_3$/MeOH 95:5 *v/v* to elute **6**. The final product was freeze-dried from benzene and was obtained as a red solid (840 mg, 95.6%). Mp 154.4 °C. Calcd for $C_{52}H_{66}N_2O_{10}$: C 71.05, H 7.57, N 3.19. Found C 70.83, H 7.03, N 3.13. EI-MS (70 eV): *m/z* 878.7 [M^+, 22.89%]. IR (ATR): ν = 2952 w, 2923 m, 2854 m, 1694 s, 1653 s, 1593 m, 1576 m, 1455 m, 1434 m, 1404 m, 1335 s, 1249 m, 1197 w, 1178 w, 1123 m, 1102 m, 1078 m, 1042 m, 1018 m, 963 w, 850 m, 808 s, 797 m, 745 s, 724 w cm^{-1}. ^1H NMR (250 MHz, $CDCl_3$, 298K): δ = 0.82 (t, J = 6.8 Hz, 6*H*, $2CH_3$), 1.10−1.45 (m, 20*H*, $10CH_2$), 1.78−1.96 (m, 2*H*, αCH_2), 2.15−2.35 (m, 2*H*, αCH_2), 3.27 (s, 6*H*, $2OCH_3$−PEG), 3.38−3.45 (m, 4*H*, $2OCH_2$−PEG), 3.51−3.80 (m, 12*H*, $6OCH_2$−PEG), 3.97 (dd, J = 10.5 Hz, J = 5.8 Hz, 2*H*, αOCH_2−OEG), 4.19 (dd, J = 10.5 Hz, J = 7.8 Hz, 2*H*, αOCH_2−OEG), 5.10−5.27 (m, 1*H*, N−CH), 5.63−5.79 (m, 1*H*, N−CH-OEG), 8.44−8.75 (m, 8*H*, 8ArH) ppm. ^{13}C NMR (62.5 MHz, $CDCl_3$, 298K): δ = 14.39 (2C, CH3), 22.94, 27.34, 29.56, 29.85, 32.13, 32.70 (12C, CH2), 52.50 (1C, N−CH-OEG), 55.11 (1C, N−CH), 59.29 (2C, OCH3-OEG), 69.64, 70.71, 70.81, 70.86, 72.18 (10C, OCH2-OEG), 123.12, 123.31, 123.63, 124.26, 126.48, 126.55, 129.73, 129.76, 131.39, 131.63, 132.16, 134.53, 134.70 (20C, CAr), 163.76 (C, CONR), 164.06 (2C, CONR-OEG), 164.86 (C, CONR) ppm.

***N*-(1-Octylheptyl)-*N*′-(2-(1,3-bis(2-(2-(2-(2-methoxyl)ethoxyl)-ethoxyl)ethoxyl)propyl))-perylene-3,4,9,10-tetracarboxylic Bisimide 7.** *N*-(1-octylhepty)-perylene-3,4,9,10-tetracarboxylic-3,4-anhydride-9,10-imide (1.2 g, 2.0 mmol) and 1,3-bis(2-(2-(2-methoxyethoxy)ethoxy)ethoxy) propane-2-amine **19d** (1.38 g, 3.6 mmol) were allowed to react according to the general procedure. The crude product was further purified by silica flash-column chromatography with $CHCl_3$/AcOH 99:1 to 9:1 *v/v* to elute impurities and then $CHCl_3$/MeOH 95:5 *v/v* to elute **7**. The final product was freeze-dried from benzene and was obtained as a red solid (1.52 g, 78.6%). Mp 148.7 °C. Calcd for $C_{56}H_{74}N_2O_{12}$: C 69.54, H 7.71, N 2.90. Found C 69.33, H 7.81, N 2.77. EI-MS (70 eV): *m/z* 966.4 [M^+, 20.18%]. IR (ATR): ν = 2956 w, 2923 m, 2855 m, 2813 w, 1694 s, 1653 s, 1593 s, 1576 m, 1506 w, 1455 w, 1435 w, 1404 m, 1337 s, 1302 m, 1250 m, 1197 w, 1178 w, 1139 m, 1102 s, 1078 m, 1034 m, 964 w, 851 m, 809 s, 797 w, 746 s, 724 w cm^{-1}. ^1H NMR (250 MHz, $CDCl_3$, 298K): δ = 0.81 (t, J = 6.8 Hz, 6*H*, $2CH_3$), 1.07−1.46 (m, 20*H*, $10CH_2$), 1.77−1.95 (m, 2*H*, αCH_2), 2.16−2.34 (m, 2*H*, αCH_2), 3.31 (s, 6*H*, $2OCH_3$−OEG), 3.44−3.77 (m, 24*H*, $12OCH_2$−OEG), 3.96 (dd, J = 10.6 Hz, J = 5.8 Hz, 2*H*, αOCH_2−OEG), 4.20 (dd, J = 10.6 Hz, J = 7.8 Hz, 2*H*, αOCH_2−OEG), 5.12−5.25 (m, 1*H*, N−CH), 5.64−5.76 (m, 1*H*, N−CH-OEG), 8.39−8.72 (m, 8*H*, 8ArH) ppm. ^{13}C NMR (62.5 MHz, $CDCl_3$, 298K): δ = 14.41 (2C, CH_3), 22.94, 27.31, 29.56, 29.85, 32.12, 32.67 (12C, CH_2), 52.35 (1C, N−CH-OEG), 55.09 (1C, N−CH), 59.33 (2C, OCH_3−OEG), 69.60, 70.64, 70.78, 70.80, 70.84, 72.18 (14C, OCH_2−OEG), 123.20, 123.37, 123.62, 124.24, 126.53, 126.59, 129.77, 131.42, 132.20, 134.59, 134.78 (20C, C_{Ar}), 163.83 (C, CONR), 164.09 (2C, CONR-OEG), 164.92 (C, CONR) ppm.

***N*-(1-Dodecylundecyl)-*N*′-(2-(1,3-bis(2-(2-(2-methoxyl)ethoxyl)-ethoxyl)propyl))-perylene-3,4,9,10-tetracarboxylic Bisimide 8.** *N*-(1-dodecylundecyl)-perylene-3,4,9,10-tetracarboxylic-3,4-anhydride-9,10-imide **12b** (714 mg, 1 mmol) and 1,3-bis(2-(2-methoxyethoxy)ethoxy) propane-2-amine (532 mg, 1.8 mmol) were allowed to react according to the general procedure. The crude product was further purified by silica flash-column chromatography with $CHCl_3$/AcOH 10:1 *v/v* to elute impurities and then $CHCl_3$/MeOH 95:5 *v/v* to elute **8**. The final product was freeze-dried from benzene and was obtained as a red solid (620 mg, 62.1%). Mp 107.7 °C. Calcd for $C_{60}H_{82}N_2O_{10}$: C 72.70, H 8.34, N 2.83. Found C 72.37, H 8.34, N 2.83. EI-MS (70 eV): *m/z* 990.1 [M^+, 25.66%]. IR (ATR): ν = 2952 w, 2921 m, 2852 m, 2817 w, 1694 s, 1653 s, 1593 s, 1576 m, 1456 w, 1434 w, 1404 m, 1338 s, 1250 m, 1197 w, 1176 w, 1107 s, 1082 m, 1018 m, 963 w, 849 m, 809 s, 795 w, 745 s, 720 w cm^{-1}. ^1H NMR (250 MHz, $CDCl_3$, 298K): δ = 0.83 (t, J = 6.8 Hz, 6*H*, $2CH_3$), 1.07−1.42 (m, 36*H*, $18CH_2$), 1.80−1.95 (m, 2*H*, αCH2), 2.18−2.33 (m, 2*H*, αCH_2), 3.27 (s, 6*H*, $2OCH_3$−OEG), 3.39−3.44 (m, 4*H*, $2OCH_2$−OEG), 3.52−3.78 (m, 12*H*, $6OCH_2$−OEG), 3.97 (dd, J = 10.6 Hz, J = 5.8 Hz, 2*H*, αOCH_2−OEG), 4.20 (dd, J = 10.6 Hz, J = 7.8 Hz, 2*H*, αOCH_2−OEG), 5.12−5.25 (m, 1*H*, N−CH), 5.65−5.77 (m, 1*H*, N−CH-OEG), 8.42−8.70 (m, 8*H*, 8ArH) ppm. ^{13}C NMR (62.5 MHz, $CDCl_3$, 298K): δ = 14.41 (2C, CH_3), 22.97, 27.33, 29.64, 29.89, 29.91, 29.94, 32.21, 32.69 (20C, CH_2), 52.50 (1C, N−CH-OEG), 55.11 (1C, N−CH), 59.28 (2C, OCH_3−OEG), 69.65, 70.71, 70.80, 70.85, 72.18 (10C, OCH_2−OEG), 123.08, 123.29, 123.59, 124.25, 126.42, 126.50, 129.68, 129.72, 131.36, 131.60, 132.14, 134.48, 134.65 (20C, C_{Ar}), 163.77 (C, CONR), 164.04 (2C, CONR-OEG), 164.86 (C, CONR) ppm.

***N*-(1-Dodecylundecyl)-*N*′-(2-(1,3-bis(2-(2-(2-(2-methoxyl)ethoxyl)-ethoxyl)ethoxyl)propyl))-perylene-3,4,9,10-tetracarboxylic Bisimide 9.** *N*-(1-dodecylundecyl)-perylene-3,4,9,10-tetracarboxylic-3,4-anhydride-9,10-imide **12b** (1.0 g, 1.4 mmol) and 1,3-bis(2-(2-(2-methoxyethoxy)ethoxy)ethoxy) propane-2-amine (970 mg, 2.5 mmol) were allowed to react according to the general procedure. The crude product was further purified by silica flash-column chromatography with $CHCl_3$/AcOH 99:1 to 9:1 *v/v* to elute impurities and then with $CHCl_3$/MeOH 95:5 *v/v* to elute **9**. The final product was freeze-dried from benzene and was obtained as a red solid (652 mg, 43.1%). Mp 111.2 °C. Calcd for $C_{64}H_{90}N_2O_{12}$: C 71.21, H 8.40, N 2.60. Found: C 70.87, H 8.67, N 2.41. EI-MS (70 eV): *m/z* 1080.3 [M^+, 34.38%]. IR (ATR): ν = 2952 w, 2921 m, 2852 m, 2813 w, 1694 s, 1654 s, 1593 s, 1576 m, 1507 w, 1456 m, 1435 m, 1404 m, 1337 s, 1251 m. 1197 w, 1180 w, 1139 m, 1104 s, 1078 m, 1030m, 963 w, 849 m, 809 s, 797 w, 746 s, 722 w cm^{-1}. ^1H NMR (250 MHz, $CDCl_3$, 298K): δ = 0.82 (t, J = 6.8 Hz, 6*H*, $2CH_3$), 1.06−1.43 (m, 36*H*, $18CH_2$), 1.78−1.94 (m, 2*H*, αCH_2), 2.16−2.34 (m, 2*H*, αCH_2), 3.31 (s, 6*H*, $2OCH_3$−OEG), 3.40−3.78 (m, 24*H*, $12OCH_2$−OEG), 3.96 (dd, J = 10.6 Hz, J = 5.8 Hz, 2*H*, αOCH_2−OEG), 4.20 (dd, J = 10.6 Hz, J = 7.8 Hz, 2*H*, αOCH_2−OEG), 5.12−5.25 (m, 1*H*, N−CH), 5.64−5.76 (m, 1*H*, N−CH-OEG), 8.36−8.78 (m, 8*H*, 8ArH) ppm. ^{13}C NMR (62.5 MHz, $CDCl_3$, 298K): δ = 14.44 (2C, CH_3), 22.99, 27.30, 29.65, 29.88, 29.92, 29.94, 32.21, 32.66 (20C, CH_2), 52.35 (1C, N−CH-OEG), 55.08 (1C, N−CH), 59.33 (2C, OCH_3−OEG), 69.60, 70.64, 70.78, 70.80, 70.84, 72.18 (14C, OCH_2−OEG), 123.20, 123.36, 123.58, 124.24, 126.53, 126.59, 129.77, 131.44, 132.18, 134.59, 134.79 (20C, C_{Ar}), 163.84 (C, CONR), 164.11 (2C, CONR-OEG), 164.91 (C, CONR) ppm.

General Procedure for the Preparation of unsymmetrical Perylene-3,4,9,10-tetracarboxylic Bisimides 5, 10, and 11 via Nucleophilic Substitution. Method A. A mixture of the respective *N*-(1-swallow-tail)-perylene-3,4,9,10-tetracarboxylic-3,4-anhydride-9,10-imide (1.0 mmol), K_2CO_3 (1.8 mmol), KI (0.2 mmol) and the respective bromide (1.8 mmol) in 20 mL absolute DMF was stirred at 80 °C for 3−7 d. The conversion was monitored via TLC or GPC. Purification procedures are described for each compound separately.

Method B. To a suspension of the respective *N*-(1-swallow-tail)-perylene-3,4,9,10-tetracarboxylic-3,4-anhydride-9,10-imide (1.0 mmol) in dry DMF (30 mL) was added NaH (1.2 mmol), as 60% suspension in mineral oil, at 0 °C. The mixture was stirred and allowed to reach RT, then the respective bromide (2.5 mmol) was added and heated to 80 °C. After 48 h, the reaction was cooled to room temperature and quenched by addition of saturated NH_4Cl solution (2.5 mL). Purification procedures are described in the corresponding compound section.

***N*-(1-Decylnonyl)-*N*′-(1-octylheptyl)-perylene-3,4,9,10-tetracarboxylic Bisimide 5.** *N*-(1-octylheptyl)-perylene-3,4,9,10-tetracarboxylic bisimide **14a** (901 mg, 1.5 mmol) and 10-bromononadecane (938 mg, 2.7 mmol) were allowed to react according to the

general procedure Method A for 7 d. After cooling to r.t., the product was precipitated in 300 mL 2N HCl/MeOH 2:1 *v/v*. After standing overnight, the precipitate was collected by filtration, washed with H_2O, then MeOH and dried at 60 °C in vacuum. The crude product was further purified by column chromatography on silica flash-gel (petrolether/$CHCl_3$ 1:1 to 1:4 *v/v*). The final product was freeze-dried from benzene and was obtained as a red solid (762 mg, 58.6%). Mp 98.8 °C. Calcd for $C_{58}H_{78}N_2O_4$: C 80.33, H 9.07 N 3.23. Found C 79.98, H 10.27, N 3.34. EI-MS (70 eV): *m/z* 866.6 ([M^+], 81.27%). IR (ATR): ν = 2956 w, 2922 m, 2853 m, 1695 s, 1651 s, 1593 s, 1578 m, 1460 w, 1434 w, 1405 m, 1335 s, 1251 m, 1209 w, 1172 m, 1124 w, 1108 w, 850 w, 809 m, 795 m, 746 m, 722 w cm^{-1}. ^1H NMR (250 MHz, $CDCl_3$, 298K): δ = 0.82 (t, J = 6.2 Hz, 12*H*, $4CH_3$), 1.10−1.42 (m, 48*H*, $24CH_2$), 1.76−1.95 (m, 4*H*, $2\alpha CH_2$), 2.14−2.35 (m, 4*H*, $2\alpha CH_2$), 5.10−5.26 (m, 2*H*, N−CH), 8.53−8.76 (m, 8*H*, 8ArH) ppm. ^{13}C NMR (62.5 MHz, $CDCl_3$, 298K): δ = 14.45, 14.48 (4C, CH_3), 23.00, 23.03, 27.36, 29.61, 29.65, 29.93, 32.18, 32.24, 32.74 (28C, CH_2), 55.14 (2C, N−CH), 123.36, 123.57, 124.28, 131.47, 132.21, 126.78, 129.95, 134.83 (20C, C_{Ar}), 163.95, 165.03 (4C, CONR) ppm.

***N*-(2-(1,3-Bis(2-(2-(2-(2-methoxyl)ethoxyl)ethoxyl)ethoxyl)propyl))-*N′*-(1-dodecyl)-perylene-3,4,9,10-tetracarboxylic Bisimide 10.** *N*-(2-(1,3-bis(2-(2-(2-(2-methoxyl)ethoxyl)ethoxyl)ethoxyl)propyl))-perylene-3,4,9,10-tetracarboxylic bisimide **14c** (946 mg, 1.25 mmol) and 12-bromododecane (561 mg, 2.25 mmol) were allowed to react according to the general procedure Method A for 3 d. After cooling to r.t. the mixture was poured into saturated NaCl solution and was extracted with $CHCl_3$. After drying over $MgSO_4$ and removal of solvent in vacuo, the crude product was further purified by column chromatography on silica flash-gel ($CHCl_3$/MeOH 98:2 *v/v*). The final product was freeze-dried from benzene to afford **10** as a dark-red solid (547 mg, 47.3%). Mp 140.1 °C. Calcd for $C_{53}H_{68}N_2O_{12}$: C 68.81, H 7.41, N 3.01. Found: C 68.99, H 7.35, N 3.03. EI-MS (70 eV): *m/z* 924.0 ([M^+], 32.38%). IR (ATR): ν = 2960 w, 2922 m, 2854 m, 2821 w, 1693 s, 1651 s, 1593s 1577 m, 1507 w, 1460 w, 1438 m, 1403 m, 1355m, 1343 s, 1249 m, 1198 w, 1180 w, 1104 s, 1030 m, 857 m, 809 s, 794 w, 745 s, 722 w cm^{-1}. ^1H NMR (250 MHz, $CDCl_3$, 298K): δ = 0.87 (s, 3*H*, CH_3), 1.12−1.53 (m, 18*H*, $9CH_2$), 1.67−1.84 (m, 2*H*, β-CH_2), 3.31 (s, 6*H*, $2OCH_3$), 3.44−3.78 (m, 24*H*, $12OCH_2$), 3.94−4.02 (dd, J = 10.5 Hz, J = 5.8 Hz, 2*H*, OEG-α-OCH_2), 4.14−4.25 (m, 4*H*, OEG-α-OCH_2, N−CH_2), 5.64−5.75 (m, 1*H*, N−CH-OEG), 8.41 (dd, J = 8.2 Hz, J = 4.4 Hz, 4*H*, $4H_{Ar}$), 8.54 (dd, J = 14.4 Hz, J = 8.0 Hz, 4*H*, $4H_{Ar}$) ppm. ^{13}C NMR (62.5 MHz, $CDCl_3$, 298K): δ = 14.45 (1C, CH_3), 23.02, 27.52, 28.46, 29.68, 29.73, 29.92, 29.97, 29.99 (9C, CH_2), 32.25 (1C, β-CH_2), 41.05 (1C, N−CH_2), 52.48 (1C, N−CH-OEG), 59.32 (2C, OCH_3−OEG), 69.66, 70.68, 70.83, 70.87, 72.21 (14C, OCH_2−OEG), 123.16, 123.22, 123.48, 123.70, 126.03, 126.45, 129.39, 129.63, 131.49, 134.51, 134.57 (20C, C_{Ar}), 163.50, 164.00 (4C, CONR) ppm.

***N*-(1-Dodecylundecyl)-*N′*-(1-(2-(2-(2-(2-methoxy)ethoxy)ethoxy)-ethoxy)ethyl)-perylene-3,4,9,10-tetracarboxylic Bisimide 11.** *N*-(1-dodecylundecyl)-perylene-3,4,9,10-tetracarboxylic bisimide **14b** (901 mg, 1.5 mmol) and 1-Bromo-tetraethyleneglycol monomethyl ether (881 mg, 3.25 mmol) were allowed to react according to the general procedure Method B for 48 h. After cooling to r.t., the product was precipitated in 300 mL 2N HCl/MeOH 3:1 *v/v*. After standing overnight, the precipitate was collected by filtration, washed with H_2O, then MeOH and dried at 60 °C in vacuum. The crude product was further purified by column chromatography on silica flash-gel (THF/hexane 1:1 *v/v*). The final product was freeze-dried from benzene and was obtained as a red solid (631 mg, 53.7%). Mp 151.8 °C. Calcd for $C_{56}H_{74}N_2O_8$: C 74.47, H 8.26, N 3.10. Found: C 74.10, H 8.90, N 3.13. EI-MS (70 eV): *m/z* 902.3 ([M^+], 87.5%). IR (ATR): ν = 2956 w, 2921 m, 2852 m, 1693 s, 1645 s, 1594 s, 1577 m, 1506 w, 1437 m, 1403 m, 1343 s, 1249 m, 1197 w, 1178 m, 1107 m, 1060 m, 1060 m, 1040 w, 857 m, 809 s, 794 m, 745 s, 720 w cm^{-1}. ^1H NMR (250 MHz, $CDCl_3$, 298K): δ = 0.84 (t, J = 6.7 Hz, 6*H*, $2CH_3$), 1.07−1.43 (m, 36*H*, $18CH_2$), 1.78−1.97 (m, 2*H*, αCH_2), 2.15−2.35 (m, 2*H*, αCH_2), 3.34 (s, 3*H*, OCH_3), 3.47−3.54 (m, 2*H*, OCH_2), 3.54−3.67 (m, 8*H*, OCH_2), 3.69−3.76 (m, 2*H*, OCH_2), 3.86 (t, J = 5.9 Hz, 2*H*, OCH_2), 4.47 (t, J = 5.9 Hz, 2*H*, N−CH_2), 5.10−5.26 (m, 1*H*, N−CH), 8.52−8.74 (m, 8*H*, 8ArH) ppm. ^{13}C NMR (62.5 MHz, $CDCl_3$, 298K): δ = 14.48 (2C, CH_3), 23.04, 27.41, 29.71, 29.96, 30.00, 32.28, 32.74 (20C, CH_2), 39.61 (1C, N−CH_2), 55.22 (1C, N−CH), 59.39 (1C, OCH_3), 68.25, 70.44, 70.86, 70.94, 71.03, 72.28 (7C, OCH_2), 123.07, 123.24, 131.41, 126.36, 129.44, 129.69, 134.31, 134.63 (20C, C_{Ar}), 163.47 (4C, CONR) ppm.

Supporting Information Available: Synthesis and characterization of perylene-intermediates. This material is available free of charge via the Internet at http://pubs.acs.org.

JA905260C